Revision 1b

Relationships among channel topology and atomic displacements in the structures of $Pb_5(BO_4)_3Cl$ with B = P (pyromorphite), V (vanadinite) and As (mimetite)

Hiroki Okudera
Earth Science Course, School of Natural System, Kanazawa University, Kanazawa, Ishikawa 920-1192, Japan
E-mail: okudera@staff.kanazawa-u.ac.jp

ABSTRACT

Rare-Earth silicate oxy-apatites have been found to exhibit high ion-conductivity along channels within their structure, which makes them candidate materials for solid oxide fuel cell electrolytes. It is not understood so far why this high ion-conductivity is restricted to oxygen transport and does not occur for halogen ions common in apatite type minerals. This study reports on the relationship between the topology of these structural channels and the spatial displacement of the chloride ion in three different structures of natural apatite group minerals [$Pb_5(BO_4)_3Cl$ (Z = 2) with B = P (pyromorphite), V (vanadinite) and As (mimetite)] using single crystal X-ray diffraction. All of these minerals crystallize in the hexagonal chlorapatite structure with space group $P6_3/m$ with no symmetry lowering or site splitting. The anion channel is built from a face-sharing array of nearly regular $Pb2_6$ octahedra running parallel to the **c**-axis, and the chloride ions were found at the center of each octahedron with bond-valence sums of 1.10 for mimetite and vanadinite, and 1.25 for pyromorphite. The mean square displacement (msd) of the chloride ion in [001] was found to be a function of the size of $Pb2_6$ octahedron in that direction. This position is also the center of a flat $O3_6$

trigonal antiprism. The msds of the chloride ion in the **xy** plane were found to be correlated to the size of the antiprism in this plane, namely the distance between the chloride ion and its nearest oxide ions, and the amount of roto-oscillation motion of the BO_4 tetrahedra around the *B*-O1 axis. While the chloride ion in the channel was bonded to six Pb cations, the repulsion from six neighboring oxygen ions is also apparent and this repulsion restricts the motion of the chloride ion within the **xy** plane.

Keywords: Pyromorphite, mimetite, vanadinite, single crystal X-ray diffraction, anion channel, apatite structure

INTRODUCTION

Studies on crystal structures and crystal-chemistry of apatite supergroup minerals and their isostructural compounds (hereafter referred as 'apatites') has had a long history since the original determination of the structure of fluorapatite by Mehmel (1930) and Náray-Szabó (1930). The discovery of high oxide-ion conductivity in rare-earth silicate oxyapatites (Nakayama et al. 1995) made their conduction mechanism a hottly debated topic in material science (e.g. Ali et al. 2009). Indeed, their excellent conductivity at relatively low temperatures is of great potential benefit in industrial applications such as electrolyte materials of solid oxide fuel cells (Fergus 2006). Since oxide-ion conductivity is dominant along [001] in these compounds (e.g. Nakayama et al. 1999), the high mobility of oxide ions within the anion channel parallel to the **c**-axis is ascribed to this high oxide-ion conductivity (e.g. Okudera et al. 2005 and references therein). Some of the authors reported improvements of conductivity with the presence of excess **oxygen** ions in the structure (e.g. Najib et al. 2004) and substitution of Si by Mg and Al (Yoshioka 2007; Kinoshita et al. 2010). The latter approach, i.e. changing the mobility of the oxygen ions by changing the topology of the channel, will be a key strategy to attain better transport property for these compounds with a

simple preparation process. However, there is no rigorous explanation why only oxygen ions in rare-earth silicate oxyapatites can move freely inside the channel while halogen anions [F^-, Cl^- and $(OH)^-$] in apatites were found to be localized at a particular position (0,0,*z*) in the channel irrespective of their ordering pattern.

The crystal structure and crystal chemistrty of those apatites are well described in recent reviews (Elliott et al. 2002; White and Zhili 2003; Pasero et al. 2010), thus only a brief summary is given here. The generalized formula of 'apatites' is written as $[A1_2][A2_3](BO_4)_3X$ ($Z = 2$) with space group $P6_3/m$, here *A*1, *A*2, *B* and *X* are designated also as atomic sites. Oxygen ions occupy two special positions O1 and O2 and one general position O3 around the *B* site. Usually, the *A*1 and *A*2 site cations at the 4*f* and 6*h* positions, respectively, are divalent, the *B* cation is pentavalent and the *X* anion monovalent. However, the apatite lattice is tolerant of substitution and charge neutrality can be maintained also by vacancies even at the *X* anion site (Elliott 1994). The description of the apatite structure can be simplified by employing a distorted hexagonal close packing model in which each sphere represents a tetrahedral $(BO_4)^{3-}$ complex anion (Fig. 1). The tetrahedral voids in this hcp model are left vacant, and octahedral voids are filled by *A*1, *A*2 and *X* ions. The occupied octahedral voids are arrayed along [001] and can be grouped into four smaller and two larger ones (per unit cell) due to a shift of the spheres within the trigonal net,. The smaller ones, i.e. 2/3 of the octahedral voids, are filled by *A*1 cations at $z \approx 0$ and $\approx 1/2$. They are coordinated by nine oxygen ions of six $(BO_4)^{3-}$ units. The remaining ones are large enough to accommodate three *A*2 cations on the distorted tringonal net (at $z = 1/4$ and 3/4). Six *A*2 cations in adjacent nets form a nearly regular trigonal antiprism with *A*2 cations on its apices. The face-sharing array of this trigonal antiprism along the **c**-axis forms an anion channel in which the *X* anion usually sits in the center of each antiprism ($z = 0$; 2*b* site with symmetry -3.. {note to typesetting, this minus sign is overbar on top of the 3 and two periods are parts of site

symmetry indication}), namely the center of the void, or the $A2_3$ regular triangle (z = 1/4; 2a, -6.. {note to typesetting, this minus sign is overbar on top of the 6 and two periods are parts of site symmetry indication}). The six oxygen ions at the O3 sites around the void also form a highly oblate trigonal antiprism by two staggered regular triangles normal to the **c**-axis with separation of 0.45 ~ 1.5 Å in the middle of each $A2_6$ trigonal antiprism (Fig. 2). Therefore, these two types of trigonal antiprism have a common center at the 2*b* site at which a chloride ion in $Pb_5(BO_4)_3Cl$ (B = P, V, As) is located. As a first report of a series of studies, the author reports here relationships between the topology of the anion channel, the size of the $O3_6$ trigonal antiprism in particular, and anisotropic displacements of chloride ion in the channel as an indication for their displacement for three natural apatite group minerals, $Pb_5(BO_4)_3Cl$ with B = P (pyromorphite), V (vanadinite) and As (mimetite) using single crystal X-ray diffraction. The position of the X anion and its stability in the channel will be subjected in the next paper of the series.

EXPERIMENTAL METHODS

Specimens

Experiments were performed on natural specimens of $Pb_5(PO_4)_3Cl$ (pyromorphite) from the Daoping Mine, Gunagxi province, China, $Pb_5(VO_4)_3Cl$ (vanadinite) from Mibladén, Morocco and $Pb_5(AsO_4)_3Cl$ (mimetite) from the Pingtouling Mine, Guangdong, China. These natural crystals occurred as long (pyromorphite, mimetite) or short (vanadinite) euhedral hexagonal prisms terminated by a basal pinacoid. Qualitative and quantitative EPMA analyses (F, Na, Al, Si, P, Cl, Ca, V, Zn, As, Sr, Ba, and Pb on a JEOL JXA-8230 operated under 15 kV, 20 nA and 100 sec. integration) indicated trace amount of impurities (Ca = 0.011 in pyromorphite, P = 0.004 in vanadinite and P = 0.012 in mimetite, with total O = 12). The results of the EPMA analyses are listed in Table 1.

Due to the pronounced anisotropy In hardness (commonly soft in [001]) the specimens were ground into an approximate sphere by hand using the Bond method. To account for shape irregularities and weak diffraction intensities, multiple data collections were performed on several specimens of the respective mineral. A total of six specimens (two per mineral with prefix OP for pyromorphite, OV for vanadinite and OM for mimetite) were ground in spheres with mean diameters around 120 μm as listed in Table 2. A somewhat larger sphere (d = 150 μm) of mimetite (OM-6) was also chosen In order to obtain better counting statistics. The results for all the specimens are used in the following discussions rather than only a selection of the best refinements based on their *R*-values.

Data collection, data treatment and structure refinements

The diffraction intensities were collected at room temperature (296 K) on a Rigaku AFC-5S automated four-circle diffractometer with graphite monochromatized Mo-Kα radiation, using the ω-2θ scan method with a scan speed of 4° per minute. The scan width was optimized for each specimen. During the data collection three standard reflections were monitored after every 200 reflections. One third of the reciprocal space (*hkl* with $0 \leq h$ and $0 \leq k$, and their Friedel pairs) was measured up to $2\theta = 90°$, and a full sphere of reciprocal space was measured for OM-6 in the same 2θ range. Relationships found among Bragg positions and intensities indicated Laue group 6/*m*. The only systematic absence of 000*l* with $l = 2n+1$ (*n*: integers) obeyed space group $P6_3/m$, and this space group was chosen. Cell dimensions were determined using 2θ values of 11 (OP-4) ~ 20 (OM-6, OV-1) most intense diffraction spots in the range of $37° < 2\theta < 50°$ and calibrated with cell dimension of Si (Okada and Tokumaru 1984).

{note to typesetting, minus sign in front of F_{obs} in this paragraph, when present, is overbar on top of the F} The measured intensities were converted to structure factors after applying Lp and spherical absorption corrections. Averages over equivalent reflections for the point group 6/*m* were taken, and some weak ($|-F_{obs}| < 3\sigma(-F_{obs})$) and ill-behaved ($|F_{obs}|_{max} > 2|F_{obs}|_{min}$ among equivalents) refelections were removed from the data sets. Only $|-F_{obs}|$ which passed the above two filters were used in the structure refinements. A weighting scheme with weights proportional to σ^{-2} was employed. The least-squares program LSGCEX (Kihara 1990) was used for structure refinements with variables including scale- and isotropic extinction factor [type I, Lorentzian mosaic spread of Becker and Coppens (1974)]. The refinements started from atomic coordinates for vanadinite given by Dai and Hughes (1989) with isotropic displacement parameters, and then the displacement parameters were expanded to anisotropic ones in subsequent iterations. Since lead chlorapatites contain pentavalent cations, atomic form factors and 2θ range for the calculations had to be carefully chosen. The lowest limit on $\sin\theta/\lambda$ was set after considering differences between neutral and ionized form factors as well as differences in refined occupancies at cation sites between neutral and ionized refinements, and their variations with respect to the minimum $\sin\theta/\lambda$ value for $|-F_{obs}|$. In these preliminary calculations site occupancies at cation sites were constrained to be equal and all the oxygen sites were assumed fully occupied. No impurities at *A*, *B* and *X* sites were introduced. The neutral form factors and anomalous dispersion terms of the atoms were taken from the International Tables for Crystallography, vol. C. The ionized form factors for Pb^{2+} and Cl^{-} were also taken from the International Tables, while values for P^{5+} and V^{5+} are from Fukamachi (1971), and O^{2-} from Raccah and Arnott (1967). Form factor for As^{5+} were not available and therefore the scattering power of the ion core of As by Fukamachi was employed. Differences in form factors were seen as negligible in $0.15 < \sin\theta/\lambda$ for Pb, $0.25 < \sin\theta/\lambda$ for P and As, and $0.40 < \sin\theta/\lambda$ for V. As a matter of fact, the

cation site occupancy converged at 100% within its esd after each refinement with the limit at 0.25, and so did the Cl site occupancy in mimetite. The Cl site occupancy converged at 96(2)% after neutral refinement of pyromorphite, and exceeded 100% in vanadinite. The latter was considered an artifact since Cl^- is the heaviest among possible *X* anion in the present case [F^-, $(OH)^-$ and Cl^-]: the anion channel site in vanadinite was fully occupied by chloride ion. In the next iterations site occupancies at each cation site were refined independently, and those converged to 100% within their esds. While the occupancy at the Cl site was still lower than unity in pyromorphite, the site is expected to be fully occupied by the chloride ion to maintain charge neutrality of the entire crystal. Selected structural parameter values in Table 3 are those after the least-squares calculations employing the neutral form factors with $|-F_{obs}|$ values in $0.25 < \sin\theta/\lambda < 0.99$ ($20.5° < 2\theta < 90°$). All the atomic sites were assumed fully occupied by respective elements and no trace elements were involved in the refinements. Variations in refined values among each preliminary and the last iterations were less than their esds. Selected interatomic distances and angles, bond-valence sums, and polyhedral volume are listed in Table 4. Mean square displacements (msds), $\langle u^2 \rangle$ ($Å^2$), of atoms are listed in Table 5.

RESULTS AND DISCUSSIONS

Structure and bond-valence sum

Results of structure refinements for these minerals involving anisotropic atomic displacement parameters (ADPs) were reported by Akao et al. (1989), Hashimoto and Matsumoto (1998) and Mills et al. (2012) for pyromorphite, Carlos et al. (1990) for mimetite and Laufek et al. (2006) for vanadinite, while no data had yet been published on anisotropy in motion for chloride ion in mimetite. The structures including anisotropic ADPs obtained here were basically identical with those previously reported: these minerals crystallized in the

chlorapatite structure with space group $P6_3/m$ and the chloride ion was found at the 2*b* position with no sign of site splitting. The Pb2 site is commonly found in off-centric coordination environment, as it has been reported for lead-containing apatites (Rouse et al. 1984; Kampf et al. 2006). The bond-valence sums (BVS) for the Pb^{2+} and *B* site cations were close to their formal valences. On the other hand the BVS values for Cl^- were around 1.10 (mimetite, vanadinite) and 1.25 (pyromorphite). Such BVS values higher than 1.25 for Cl^- were found also in phosphohedyphane ($Ca_2Pb_3(PO_4)_3Cl$, Kampf et al. 2006), $Sr_2Ba_3(AsO_4)_3Cl$ (Đordević et al. 2008), synthetic alforsite ($Ba_5(PO_4)_3Cl$, Hata et al. 1979), and lower than 1.1 in $Sr_5(VO_4)_3Cl$ (Beck et al. 2006). This variation on BVS, namely the volume of $A2_6$ octahedron, indicate that the structure is less dependent of the size of *X* anion.

Anisotropic motions of BO_4 tetrahedron

The msds at the *B* site were the smallest among the corresponding atomic sites in these type of compounds. Anisotropy in msds was prominent at the O sites, and the minimum of msds at each O site was found approximately In direction of the *B*-O bond. In mimetite and vanadinite the displacement ellipsoid at the O1 site Is an oblate spheroid, and those at the other three oxygen sites (1 x O2, 2 x O3) were highly prolate. At the O2 and O3 sites the principal axes for the maximum amplitudes were found as tangents of the circle, which inscriped O3-O2-O3' triangle. These msds at the *B* and O sites indicated mostly roto-oscillation motion of BO_4 around the *B*-O1 axis with a virtually fixed center of gravity at the *B* site. This anisotropy could be seen also on pyromorphite, though not as apparent as in the other two phases. When the $(BO_4)^{3-}$ complex ion is roto-oscillating around the *B*-O1 axis, O2 and O3 oxygen ions are moving on the above mentioned circle. If this is the case, the gravity-center of atomic PDF (obtained as an atomic position in a harmonic refinement) at O2 and O3 sites move toward the center of the circle and the O1-*B*-O2 and O1-*B*-O3 angles

are calculated larger than the value for regular tetrahedron (109.47°). In reality, six O-*B*-O angles were divided into two groups; the O-*B*-O angles involving the O1 site were close to each other and larger than the ideal value, and the other three were also close to each other but smaller than the ideal value, in all specimens. Variations on bond angle variances, $\sigma_{\theta(tet)}^2$ (Robinson et al. 1971), were smaller in pyromorphite and larger in vanadinite and mimetite. There magnitude is compatible with the anisotropy of the msds at the O2 and O3 sites. The same atomic motions and angle variations on BO_4 tetrahedron were found also on phosphohedyphane (Kampf et al. 2006), hydroxylapatite ($Ca_5(PO_4)_3OH$, Sudarsanan and Young 1969) and most of the Sr-bearing apatites hitherto published (e.g. Sudarsanan and Young 1972, 1974; Rakovan and Hughes 2000; Đordević et al. 2008).

This roto-oscillation motion around *B*-O1, however, is not mandatory for the structure. In rare-earth silicate oxyapatites highly prolate displacement ellipsoids were found at the O1 and O3 sites and their longest principal axes were virtually on longitude lines of the BO_4 sphere with O2 site as a pole (Okudera et al. 2004, 2005). This mode was also apparent in $Ba_5(VO_4)_3Cl$ (Roh and Hong 2005) and synthetic turneaureite ($Ca_5(AsO_4)_3Cl$, Wardojo and Hwu 1996). The cause of this difference is beyond the scope of this paper and it is an open question for studies in the future.

Displacements of chloride ion and their anisotropy

In all of the present specimens the chloride ion is positioned in the center of the $Pb2_6$ trigonal antiprism, and these antiprisms are fairly close to a regular octahedron with a little (pyromorphite, mimetite), or virtually no (vanadinite), prolongation along [001]. Under such circumstances, msds at the Cl site are expected to be virtually isotropic, and the amplitudes of those displacements are expected to be a simple function of the size of $Pb2_6$ octahedron. The msd along [001] followed this assumption: the msd in [001] and size of the octahedron along

the direction (= c/2 Å) were 0.016-0.019 Å^2 and 3.67 Å for vanadinite, 0.017 Å^2 and 3.68 Å for pyromorphite, and 0.022-0.023 Å^2 and 3.72-3.73 Å for mimetite. The differences among values for vanadinite and pyromorphite were less than the present experimental precision, but the values for mimetite were apparently larger than those in the others. This relationship, however, did not hold in the **xy** plane. Instead of considering the circles inscribing or circumscribing the antiprism at z = 0, the area of the $Pb2_3$ triangle was used as a qualitative measure of the size of the octahedron in the **xy** plane at z = 0. The area increased in the order of pyromorphite (8.19-8.22 Å^2), mimetite (8.43-8.44 Å^2) and vanadinite (8.59 Å^2), while the msds at the Cl site in the **xy** plane increased in a different order, namely pyromorphite (0.017 Å^2), vanadinite (0.019-0.021 Å^2) and mimetite (0.022-0.025 Å^2).

One of the parameters which followed the latter order was the size of the $O3_6$ trigonal antiprism in the **xy** plane. As it can be seen in Figure 2(b), the antiprism is composed of two regular triangles normal to the **c**-axis with a narrow gap. When we set spheres of 1.26 Å radius (crystal ionic radius for O^{2-} by Shannon, 1976) at the apices of the $O3_6$ antiprism and employed the radius r of the inscribing sphere as a measure, the size of the antiprism in the **xy** plane was the smallest in pyromorphite (r = 2.05 Å) and practically the same in mimetite (r = 2.12-2.14 Å) and vanadinite (r = 2.12 Å). It is worth to note that these radii are close to the crystal ionic radius for Cl^- (1.67 Å) by Shannon (1976), and the repulsion between oxygen and chloride ions should be considered in this discussions. Another parameter was the maximum msd at the O3 site. As it is shown in Figure 3, the Cl site is surrounded by six O3-O2-O3' triangles of six $(BO_4)^{3-}$ spheres which form an octahedral void in the hexagonal close packing. These triangles were normal to the **xy** plane and were arranged as if they were nearly bisecting the channel. Under such an arrangement, a rotating motion of the O3-O2-O3' triangle causes the O3 site to push the chloride ion to the other side within the **xy** plane. The maxima of msds at the O3 site, pyromorphite (0.03-0.04 Å^2),

vanadinite (0.05-0.06 $Å^2$) and mimetite (0.13-0.15 $Å^2$), followed the increasing order of the msd at the Cl site in the **xy** plane. While chloride ion in the channel was bound to six Pb2 cations, the repulsion from the neighboring six oxygen ions Is also apparent, and this repulsion restricts the motion of the chloride ion in the **xy** plane.

ACKNOWLEDGEMENTS

The author thanks to Dr. Y. Kamiyama of JEOL for EPMA measurements.

REFERENCES CITED

Akao, A., Aoki, H., Innami, Y., Minamikata, S., and Yamada, T. (1989) Flux growth and crystal structure of pyromorphite. Reports of the Institute for Medical and Dental Engineering, Tokyo Medical and Dental University, 23, 25-29.

Ali, R., Yashima, M., Matsushita, Y., Yoshioka, H., and Izumi, F. (2009) Crystal structure and electron density in the apatite-type ionic conductor $La_{9.71}(Si_{5.81}Mg_{0.18})O_{26.37}$. Journal of Solid State Chemistry, 182, 2846-2851.

Beck, H.P., Douiheche, M., Haberkorn, R., and Kohlmann, H. (2006) Synthesis and characterisation of chloro-vanadato-apatites $M_4(VO_4)_3Cl$ (M = Ca, Sr, Ba). Solid State Sciences, 8, 64-70.

Becker, P.J. and Coppens, P. (1974) Extinction within the limit of validity of the Darwin transfer equations. I. General formalisms for primary and secondary extinction and their application to spherical crystals. Acta Crystallographica, A30, 129-147.

Brese, N.E. and O'Keeffe, M. (1991) Bond-valence parameters for solids. Acta Crystallographica, B47, 192-197.

Brown, I.D. and Altermatt, D. (1985) Bond-valence parameters obrtained from a systematic analysis of the inorganic crystal structure database. Acta Crystallographica, B41, 244-247.

Calos, N.J., Kennard, C.H.L., and Davis, R.L. (1990) Crystal structure of mimetite, $Pb_5(AsO_4)_3Cl$. Zeitschrift für. Kristallographie, 191, 125-129.

Dai, Y. and Hughes, J.M. (1989) Crystal-structure refinements of vanadinite and pyromorphite. Canadian Mineralogist, 27, 189-192.

Đordević, T., Šutović, S., Stojanović, J., and Karanović, L. (2008) Sr, Ba and Cd arsenates with the apatite-type structure. Acta Crystallographica, C64, i82-i86.

Elliott, J.C. (1994) Structure and Chemistry of the apatites and other calcium orthophosphates. Studies in Inorganic Chemistry, 18, 404 p. Elsevier, Amsterdam.

Elliott, J.C., Wilson, R.M., and Dowker, S.E.P. (2002) Apatite structures. Advances in X-ray Analysis, 45, 172-181.

Fergus, J.W. (2006) Electrolytes for solid oxide fuel cells. Journal of Power Sources, 162, 30-40.

Fukamachi, T. (1971) Mean X-ray scattering factors calculated from analytical Roothaan-Hartree-Fock wave functions by Clementi. Technical Report of ISSP, Series B, no. 12.

Hashimoto, H. and Matsumoto, T. (1998) Structure refinements of two natural pyromorphites, $Pb_5(PO_4)_3Cl$, and crystal chemistry of chlorapatite group, $M_5(PO_4)_3Cl$. Zeitschrift für Kristallographie, 213, 585-590.

Hata, M., Marumo, F., and Iwai, S. (1979) Structure of barium chlorapatite. Acta Crystallographica, B35, 2382-2384.

296 Kampf, A.R., Steele, I.M., and Jenkins, R.A. (2006) Phosphohedyphane, $Ca_2Pb_3(PO_4)_3Cl$, the
297 phosphate analogue of hedyphane: Description and crystal structure. American
298 Mineralogist, 91, 1909-1917.
299 Kihara, K. (1990) An X-ray study of the temperature dependence of the quartz structure.
300 European Journal of Mineralogy, 2, 63-77.
301 Kinoshita, T., Iwata, T., Béchade, E., Masson, O., Julien, I., Champion, E., Thomas, P.,
302 Yoshida, H., Ishizawa, N., and Fukuda, K. (2010) Effect of Mg substitution on
303 crystal structure and oxide-ion conductivity of apatite-type lanthanum silicates. Solid
304 State Ionics, 181, 1024-1032.
305 Krivovichev, S.V. and Brown, I.D. (2001) Are the compressive effects of encapsulation an
306 artifact of the bond valence parameters? Zeitschrift für Kristallographie, 216,
307 245-247.
308 Laufek, F., Skála, R., Haloda, J., and Císařová, I. (2006) Crystal structure of vanadinite:
309 Refinement of anisotropic displacement parameters. Journal of the Czech Geological
310 Society, 51, 271-275.
311 Mackie, P.E., Elliott, J.C., and Young, R.A. (1972) Monoclinic structure of synthetic
312 $Ca_5(PO_4)_3Cl$, chlorapatite. Acta Crystallographica, B28, 1840-1848.
313 Mehmel, M. (1930) Über die Structur des Apatites. I. Zeitschrift für Kristallographie, 75,
314 323-331.
315 Mills, S.J., Ferraris, G., Kampf, A.R., and Favreau, G. (2012) Twinning in pyromorphite: The
316 first documented occurrence of twinning by merohedry in the apatite supergroup.
317 American Mineralogist, 97, 415-418.
318 Momma, K. and Izumi, F. (2008) VESTA: a three-dimensional visualization system for
319 electronic and structural analysis. Journal of Applied Crystallography, 41, 653-658.

Najib, A., Sansom, H.E.H., Tolchard, J.R., Slater, P.R., and Islam, M.S. (2004) Doping strategies to optimise the oxide ion conductivity in apatite-type ionic conductors. Dalton Transaction, 3106-3109.

Nakayama, S., Kageyama, T., Aono, H., and Sadaoka, Y. (1995) Ionic-conductivity of lanthanoid silicates, $Ln_{10}(SiO_4)_6O_3$ (Ln = La, Nd, Sm, Gd, Dy, Y, Ho, Er, and Yb). Journal of Materials Chemistry, 5, 1801-1805.

Nakayama, S., Sakamoto, M., Higuchi, M., Kodaira, K., Sato, M., Kakita, S., Suzuki, T., and Itoh, K. (1999) Oxide ionic conductivity of apatite type $Nd_{9.33}(SiO_4)_6O_2$ single crystal. Journal of the European Ceramic Society, 19, 507-510.

Náray-Szabó, St. (1930) The structure of apatite $(CaF)Ca_4(PO_4)_3$. Zeitschrift für Kristallographie, 75, 387-398.

Okada, Y. and Tokumaru, Y. (1984) Precise determination of lattice parameters and thermal expansion coefficient of silicon between 300 and 1500 K. Journal of Applied Physics, 56, 314-320.

Okudera, H., Yoshiasa, A., Masubuchi, Y., Higuchi, M., and Kikkawa, S. (2004) Determinations of crystallographic space group and atomic arrangements in oxide-ion-conducting $Nd_{9.33}(SiO_4)_6O_2$. Zeitschrift für Kristallographie, 219, 27-31.

Okudera, H., Masubuchi, Y., Kikkawa, S., and Yoshiasa, A. (2005) Structure of oxide ion-conducting lanthanum oxyapatite, $La_{9.33}(SiO_4)_6O_2$. Solid State Ionics, 176, 1473-1478.

Pasero, M., Kampf, A.R., Ferraris, C., Pekov, I.V., Rakovan, J., and White, T.J. (2010) Nomenclature of the apatite supergroup minerals. European Journal of Mineralogy, 22, 163-179.

Raccah, P.M. and Arnott, R.J. (1967) Comparison of the theoretical O^{--} form factors with experiment. Physical Review, 153, 1028-1031.

Rakovan, J.F. and Hughes, J.M. (2000) Strontium in the apatite structure: Strontian fluorapatite and belovite-(Ce). Canadian Mineralogist, 38, 839-845.

Robinson, K., Gibbs, G.V., and Ribbe, P.H. (1971) Quadratic elongation: A quantitative measure of distortion in coordination polyhedra. Science, 172, 567-570.

Roh, Y. and Hong, S. (2005) Apatite-type $Ba_5(VO_4)_3Cl$. Acta Crystallographica, E61, i140-i142.

Rouse, R.C., Dunn, P.J., and Peacor, D.R. (1984) Hedyphane from Franklin, New Jersey and Långban, Sweden: cation ordering in an arsenate apatite. American Mineralogist, 69, 920-927.

Shannon, R.D. (1976) Revised effective ionic radii and systematic studies of interatomic distances in halides and chalcogenides. Acta Crystallographica, A32, 751-767.

Sudarsanan, K. and Young, R.A. (1969) Significant precision in crystal structural details: Holly Springs hydroxyapatite. Acta Crystallographica, B25, 1534-1543.

Sudarsanan, K. and Young, R.A. (1972) Structure of strontium hydroxide phosphate, $Sr_5(PO_4)_3OH$. Acta Crystallographica, B28, 3668-3670.

Sudarsanan, K. and Young, R.A. (1974) Structure refinement and random error analysis for strontium 'chlorapatite', $Sr_5(PO_4)_3Cl$. Acta Crystallographica, B30, 1381-1386.

Wardojo, T.A. and Hwu, S. (1996) Chlorapatite: $Ca_5(AsO_4)_3Cl$. Acta Crystallographica, C52, 2959-2960.

White T. J. and ZhiLi, D. (2003) Structural derivation and crystal chemistry of apatites. Acta Crystallographica, B59, 1-16.

Yoshioka, H. (2007) Enhancement of ionic conductivity of apatite-type lanthanum silicates doped with cations. Journal of the American Ceramic Society, 90, 3099-3105.

FIGURE CAPTIONS

370

371 FIGURE 1. Schematic illustration of hexagonal chlorapatite structure as a stack of trigonal
372 nets in a hcp manner. One unit cell is shown as rhombus. (a) Undistorted stacking of the
373 trigonal nets of $(BO_4)^{3-}$complex anion at z = 1/4 and 3/4. *A*1 cations and chloride anions
374 occupy centers of the octahedral voids of the packing. (b) Distorted (real) trigonal nets. These
375 nets are distorted in-plane and are still at the same hight as in (a). In the end-member
376 chlorapatite, $Ca_5(PO_4)_3Cl$, the chloride ion slightly moves along the **c**-axis and the crystal
377 symmetry is lowered to monoclinic with a doubled cell (Mackie et al. 1972). Gray spheres:
378 *A*1 cations, black spheres: *A*2 cations, pale-gray spheres: $(BO_4)^{3-}$complex anion, open circles:
379 chloride ions. Oxygen ions are not shown for clarity.

380

381 FIGURE 2. (a) ORTEP drawing of vanadinite (OV-5) structure with 70% probability
382 ellipsoids. (b) Construction of an anion channel running through the structure along the **c**-axis.
383 Only Pb2, O3 and Cl are shown with 70% probability ellipsoids. Figures 2 and 3 were all
384 drawn with VESTA (Momma and Izumi 2008)

385

386 FIGURE 3. Top view of the coordination environment of Cl by six $(AsO_4)^{3-}$ complexes in
387 mimetite (OM-3) structure. As-O bonds are drawn with gray lines. O3-O2-O3' triangles
388 (normal to the **xy** plane) are drawn with solid lines.

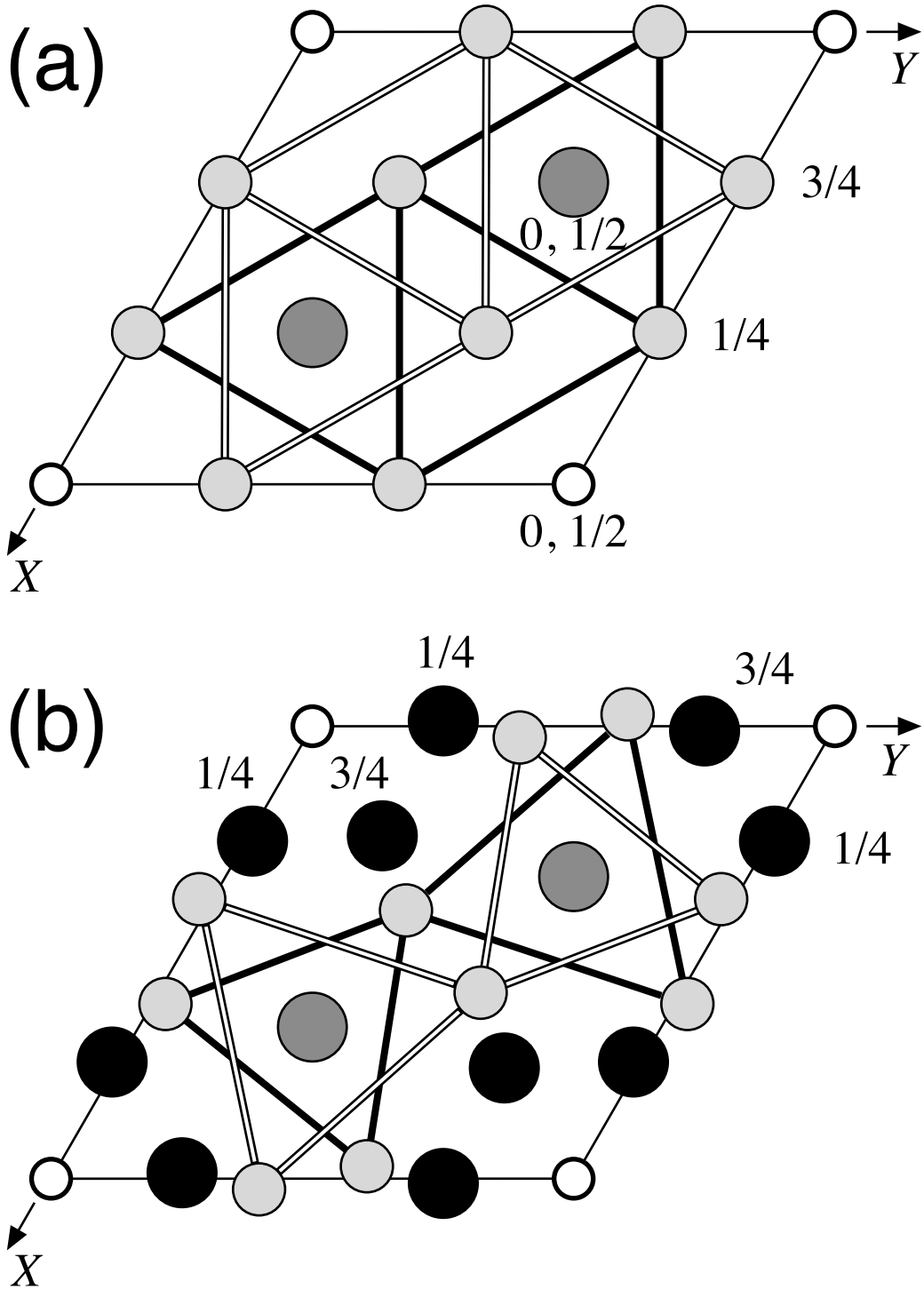

Okudera Figure 1 (200%)

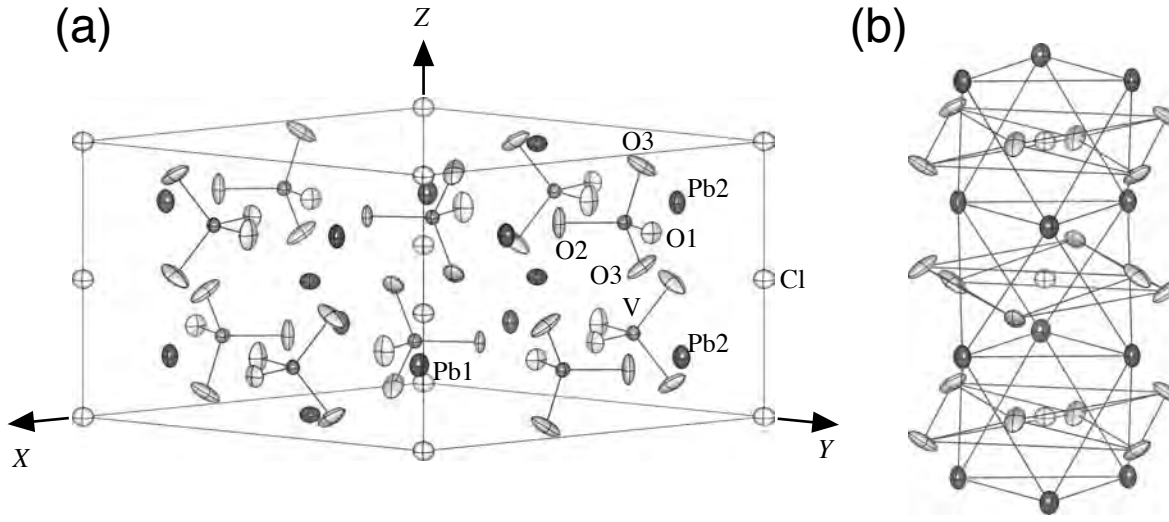

Okudera Figure 2 (100%)

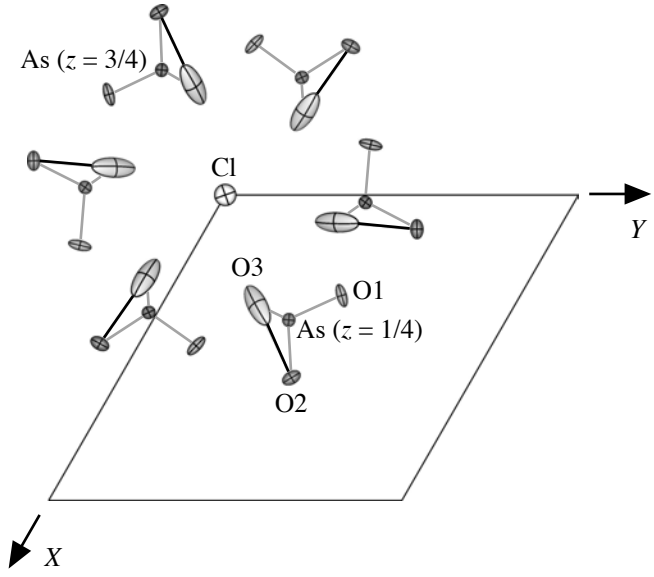

Okudera Figure 3 (100%)

TABLE 1. Mean compositions (wt%) of the subjected minerals based on O = 12 afpu

	Pyromorphite		Vanadinite		Mimetite	
	mass	atom	mass	atom	mass	atom
CaO	0.049	0.011	n.d.	n.d.	n.d.	n.d.
PbO	81.381	4.697	78.159	4.511	73.657	4.993
As2O5	n.d.	n.d.	0.018	0.002	21.074	2.774
P2O5	16.050	2.913	0.067	0.012	0.109	0.023
V2O5	n.d.	n.d.	21.008	2.976	n.d.	n.d.
Cl	2.861	0.956	2.725	0.915	2.562	1.001
=O	-0.646		-0.615		-0.578	
total	99.695	8.577	101.362	8.416	96.842	8.791

Standards: wollastonite (Ca), crocoite (Pb), cobaltite (As), fluorapatite (P), synthetic V_2O_5 (V), and tugtupite (Cl)
n.d.: zero within 1σ

TABLE 2. Crystallographic data and details of structure refinements

Mineral	Pyromorphite		Vanadinite		Mimetite	
Formula (EPMA)	$Pb_{4.697}Ca_{0.011}(P_{0.971}O_4)_3Cl_{0.956}$		$Pb_{4.511}(As_{0.0007}P_{0.004}V_{0.992}O_4)_3Cl_{0.915}$		$Pb_{4.993}(As_{0.925}P_{0.012}O_4)_3Cl_{1.001}$	
Formula weight (EPMA, amu)	1290.3		1311.2		1471.0	
Formula (employed)	$Pb_5(PO_4)_3Cl$		$Pb_5(VO_4)_3Cl$		$Pb_5(AsO_4)_3Cl$	
Space group	$P6_3/m$		$P6_3/m$		$P6_3/m$	
Specimen	OP-1	OP-4	OV-1	OV-5	OM-3	OM-6
a (Å)	9.986(1)	9.979(1)	10.3231(9)	10.322(1)	10.238(1)	10.240(1)
c (Å)	7.338(1)	7.344(1)	7.3399(7)	7.341(1)	7.450(1)	7.441(2)
Volume	633.6(2)	633.3(3)	677.4(2)	677.3(3)	676.3(3)	675.6(4)
Z	2	2	2	2	2	2
Density, calculated	7.11	7.11	6.94	6.94	7.31	7.32
Radiation type and wavelength	Mo Kα, λ = 0.71069 Å					
Absorption coefficient (mm^{-1})	66.97	67.00	64.23	64.24	69.68	69.75
Crystal diameter (mean, mm)	0.126	0.120	0.116	0.116	0.118	0.150
μr for spherical absorption correction	4.219	4.020	3.725	3.726	3.895	5.231
Max. fluctuation in $\|F_{obs}\|$ on 360° ψ-scan	± 7%	± 3%	± 12%	± 7%	± 7%	± 6%
Diffractometer	Rigaku AFC-5S					
Data collection method and scan speed	ω-2θ scan, 4°/min					
2θ range collected	2θ ≤ 90°					
Reciprocal space	*hkl* of 0 ≤ *h* and 0≤ *l*, and their Friedel equivalent reflections, total 1/3 sphere					all sphere
Reflections collected	7834	7823	8324	8316	8100	22334
Independent reflections	1856	1858	1979	1977	1959	1961
Number of parameters	40					
2θ range used	20.5° ~ 90°					
Independent reflections used	848	797	641	707	730	607
R_{int} (%) used	4.03	3.90	4.77	4.56	4.38	4.94
R (%)	2.58	2.39	3.05	3.14	3.47	2.29
w*R* (%)	2.76	2.45	2.87	3.04	3.56	2.60
Goodness of fit on F	0.56	0.51	0.54	0.58	0.68	0.55

TABLE 3. Extinction factor, atomic coordinates and anisotropic displacement parameters

		OP-1	OP-4	OV-1	OV-5	OM-3	OM-6
Extinction factor		0.071(6)	0.069(6)	0.058(6)	0.060(7)	0.062(8)	0.034(5)
Site		Coordinates and atomic displacement parameters (Å^2)					
Pb1	x	1/3	1/3	1/3	1/3	1/3	1/3
	y	2/3	2/3	2/3	2/3	2/3	2/3
	z	0.00476(8)	0.00470(7)	0.00771(10)	0.00784(10)	0.0069(1)	0.0676(9)
	U_{11}	0.0177(1)	0.0173(1)	0.0184(2)	0.0195(2)	0.0200(2)	0.0213(2)
	U_{33}	0.0100(1)	0.0091(1)	0.0088(2)	0.0122(2)	0.0085(3)	0.0138(2)
Pb2	x	0.25478(4)	0.25448(4)	0.25496(6)	0.25502(6)	0.25106(7)	0.25078(6)
	y	0.00599(4)	0.00580(4)	0.01228(6)	0.01233(6)	0.00419(7)	0.00402(6)
	z	1/4	1/4	1/4	1/4	1/4	1/4
	U_{11}	0.0106(1)	0.0104(1)	0.0119(2)	0.0128(2)	0.0107(2)	0.0121(2)
	U_{22}	0.0131(1)	0.0133(1)	0.0163(2)	0.0180(2)	0.0144(2)	0.0150(2)
	U_{33}	0.0244(2)	0.0237(2)	0.0220(2)	0.0261(2)	0.0353(4)	0.0402(3)
	U_{12}	0.0054(1)	0.0055(1)	0.0069(2)	0.0076(2)	0.0062(2)	0.0070(2)
B	x	0.4105(3)	0.4100(3)	0.4094(2)	0.4094(2)	0.4096(2)	0.4091(1)
	y	0.3794(3)	0.3795(3)	0.3837(2)	0.3838(2)	0.3846(2)	0.3845(1)
	z	1/4	1/4	1/4	1/4	1/4	1/4
	U_{11}	0.0092(8)	0.0082(7)	0.0103(8)	0.0105(7)	0.0087(5)	0.0094(4)
	U_{22}	0.0080(8)	0.0066(7)	0.0079(8)	0.0102(7)	0.0073(5)	0.0084(4)
	U_{33}	0.0082(8)	0.0098(8)	0.0072(8)	0.0100(8)	0.0094(5)	0.0145(5)
	U_{12}	0.0046(7)	0.0037(6)	0.0051(7)	0.0056(6)	0.0039(4)	0.0046(4)
O1	x	0.3416(10)	0.3435(10)	0.3345(14)	0.3309(11)	0.3306(14)	0.3293(12)
	y	0.4874(9)	0.4887(10)	0.4991(13)	0.4966(11)	0.4953(13)	0.4942(11)
	z	1/4	1/4	1/4	1/4	1/4	1/4
	U_{11}	0.024(3)	0.027(4)	0.033(6)	0.020(4)	0.019(5)	0.027(5)
	U_{22}	0.014(3)	0.021(3)	0.024(5)	0.016(4)	0.013(4)	0.018(4)
	U_{33}	0.016(3)	0.019(3)	0.010(4)	0.022(5)	0.022(6)	0.026(5)
	U_{12}	0.015(3)	0.019(3)	0.022(5)	0.015(4)	0.009(4)	0.019(4)
O2	x	0.5890(9)	0.5891(9)	0.6013(12)	0.6019(10)	0.5978(16)	0.5986(12)
	y	0.4742(9)	0.4743(9)	0.4862(14)	0.4859(12)	0.4860(17)	0.4866(12)
	z	1/4	1/4	1/4	1/4	1/4	1/4
	U_{11}	0.010(2)	0.011(3)	0.009(4)	0.008(4)	0.016(6)	0.011(4)
	U_{22}	0.010(3)	0.013(3)	0.018(5)	0.017(5)	0.019(6)	0.011(4)
	U_{33}	0.030(4)	0.034(4)	0.033(7)	0.045(7)	0.081(14)	0.097(12)
	U_{12}	0.002(2)	0.004(2)	0.000(4)	0.002(3)	0.009(5)	0.001(3)
O3	x	0.3611(8)	0.3615(7)	0.3600(11)	0.3589(10)	0.3635(18)	0.3617(16)
	y	0.2741(8)	0.2728(7)	0.2698(12)	0.2701(10)	0.2743(18)	0.2721(16)
	z	0.0806(10)	0.0815(9)	0.0642(14)	0.0663(12)	0.072(2)	0.0698(18)
	U_{11}	0.032(3)	0.020(2)	0.037(5)	0.040(4)	0.074(9)	0.089(9)
	U_{22}	0.023(2)	0.020(2)	0.035(4)	0.036(4)	0.067(8)	0.082(8)
	U_{33}	0.019(3)	0.019(2)	0.021(4)	0.023(4)	0.051(7)	0.054(6)
	U_{12}	0.017(2)	0.009(2)	0.027(4)	0.028(4)	0.059(8)	0.075(8)
	U_{13}	-0.012(2)	-0.010(2)	-0.018(4)	-0.022(3)	-0.051(7)	-0.056(6)
	U_{23}	-0.010(2)	-0.011(2)	-0.014(4)	-0.017(3)	-0.052(7)	-0.056(6)
Cl	x	0	0	0	0	0	0
	y	0	0	0	0	0	0
	z	0	0	0	0	0	0
	U_{11}	0.0167(9)	0.0166(8)	0.0191(14)	0.0211(13)	0.0217(17)	0.0253(14)
	U_{33}	0.017(2)	0.017(2)	0.017(3)	0.019(3)	0.023(3)	0.022(3)

Note: $U_{22} = U_{11}$ and $U_{12} = 1/2U_{11}$ at Pb1 and Cl sites, $U_{13} = U_{23} = 0$ at Pb1, Pb2, *B*, O1, O2 and Cl sites

TABLE 4. Selected interatomic distances, bond angles, polyhedral volume and bond-valence sums

Bond		Distances (Å), angles (°), bond-valence sums and polyhedral volume (Å^3)					
		OP-1	OP-4	OV-1	OV-5	OM-3	OM-6
Pb1 site							
Pb1-O1	[x 3]	2.569(7)	2.567(7)	2.485(11)	2.489(9)	2.512(11)	2.515(9)
Pb1-O2	[x 3]	2.677(7)	2.677(7)	2.755(12)	2.750(10)	2.776(15)	2.774(10)
Pb1-O3	[x 3]	2.872(9)	2.863(8)	2.942(13)	2.957(12)	2.91(2)	2.917(18)
Mean value		2.706(8)	2.703(8)	2.727(12)	2.732(10)	2.733(16)	2.735(12)
Bond-valence sum		2.04	2.05	2.04	2.02	1.98	1.97
Pb2 site							
Pb2-O1		3.075(10)	3.089(10)	3.217(15)	3.183(12)	3.082(15)	3.070(13)
Pb2-O2		2.359(8)	2.359(9)	2.330(13)	2.332(12)	2.344(16)	2.341(11)
Pb2-O3	[x 2]	2.646(7)	2.650(7)	2.686(11)	2.683(10)	2.747(17)	2.739(15)
Pb2-O3'	[x 2]	2.639(8)	2.632(6)	2.574(12)	2.582(11)	2.639(18)	2.615(16)
Pb2-Cl	[x 2]	3.1128(5)	3.1106(5)	3.1586(6)	3.1588(6)	3.1572(7)	3.1544(6)
Mean value		2.778(6)	2.779(6)	2.798(9)	2.795(8)	2.814(13)	2.804(11)
Bond-valence sum		1.96	1.97	1.95	1.95	1.83	1.88
B site							
B-O1		1.542(12)	1.533(12)	1.714(17)	1.720(14)	1.690(17)	1.687(14)
B-O2		1.545(8)	1.548(8)	1.717(10)	1.721(9)	1.671(14)	1.682(10)
B-O3	[x 2]	1.541(7)	1.544(6)	1.704(10)	1.690(9)	1.648(16)	1.673(14)
Mean value		1.542(8)	1.542(8)	1.710(12)	1.705(10)	1.664(16)	1.679(13)
Bond-valence sum		4.90	4.89	5.15	5.22	5.28	5.08
O1-*B*-O2		110.6(5)	110.0(5)	110.7(7)	112.1(6)	111.9(8)	112.2(6)
O1-*B*-O3	[x 2]	112.0(4)	113.1(4)	113.4(6)	112.6(5)	113.0(9)	112.8(8)
O2-*B*-O3	[x 2]	107.2(4)	106.8(3)	106.3(4)	106.6(4)	105.8(7)	106.0(6)
O3-*B*-O3'		107.6(4)	106.6(3)	106.3(5)	105.9(4)	106.9(8)	106.5(7)
bond-angle variance		5.65	9.76	12.4	11.1	12.8	12.6
Cl site in $Pb2_6$							
Polyhedral volume		40.188(7)	40.101(6)	42.015(10)	42.020(9)	41.929(11)	41.820(9)
Bond-valence sum		1.24	1.25	1.10	1.10	1.10	1.11
Area of regular $Pb2_3$		8.215(3)	8.191(3)	8.586(3)	8.586(4)	8.442(5)	8.431(4)
Cl site in $O3_6$							
Cl-O3		3.313(11)	3.311(9)	3.382(12)	3.377(11)	3.402(20)	3.381(12)
Area of regular $O3_3$		13.80(5)	13.78(5)	14.70(10)	14.51(10)	14.66(15)	14.50(15)

Note: bond valence parameters were taken from Krivovichev and Brown (2001) for Pb^{2+}-O^{2-}, Brese and O'Keeffe (1991) for Pb^{2+}-Cl^{-}, and Brown and Altermatt (1985) for the others.

TABLE 5. Mean square displacements, $<u^2>$, of atoms along three principal axes

		OP-1	OP-4	OV-1	OV-5	OM-3	OM-6
Site		$<u^2>$ (Å^2)					
Pb1*	[001]	0.0100(1)	0.0090(1)	0.0088(2)	0.0123(2)	0.0085(3)	0.0138(2)
	XY	0.01771(7)	0.01733(7)	0.01836(11)	0.01949(11)	0.01995(12)	0.0213(1)
Pb2	Min	0.0106(1)	0.0104(1)	0.0116(3)	0.0125(3)	0.0104(3)	0.0117(2)
		0.0138(2)	0.0139(2)	0.0167(3)	0.0185(3)	0.0147(3)	0.0151(2)
	Max	0.0244(2)	0.0237(2)	0.0220(2)	0.0261(2)	0.0353(4)	0.0402(3)
B site	Min	0.0076(12)	0.0065(9)	0.0071(12)	0.0095(14)	0.0073(6)	0.0082(5)
		0.0082(8)	0.0083(9)	0.0072(8)	0.0100(8)	0.0089(7)	0.0094(5)
	Max	0.0092(7)	0.0098(8)	0.0103(8)	0.0107(5)	0.0094(5)	0.0145(5)
O1	Min	0.005(5)	0.009(7)	0.010(4)	0.005(8)	0.011(7)	0.005(8)
		0.016(3)	0.019(3)	0.012(10)	0.022(5)	0.018(5)	0.026(5)
	Max	0.025(3)	0.029(3)	0.035(4)	0.022(3)	0.022(6)	0.029(3)
O2	Min	0.008(2)	0.010(2)	0.007(3)	0.008(3)	0.016(7)	0.008(2)
		0.015(5)	0.016(5)	0.030(9)	0.023(7)	0.020(8)	0.020(7)
	Max	0.030(4)	0.034(4)	0.033(7)	0.045(7)	0.081(14)	0.097(12)
O3	Min	0.010(2)	0.007(2)	0.009(4)	0.008(4)	0.006(7)	0.010(6)
		0.020(5)	0.022(4)	0.020(8)	0.020(7)	0.023(16)	0.021(15)
	Max	0.040(2)	0.032(2)	0.053(3)	0.059(3)	0.131(6)	0.150(5)
Cl*	[001]	0.0171(16)	0.0173(16)	0.017(3)	0.019(3)	0.023(3)	0.022(3)
	XY	0.0167(9)	0.0166(5)	0.0191(9)	0.0211(13)	0.0218(11)	0.0253(14)

* One of the principal axes is parallel to the *c*-axis and the other two in the *XY* plane are identical due to site symmetry